Immobilization of Quantum Dots *via* Conjugated Self-Assembled Monolayers and Their Application as a Light-Controlled Sensor for the Detection of Hydrogen Peroxide

Waqas Khalid,[†,§] Mira El Helou,[†,§] Tobias Murböck,[†] Zhao Yue,[†,∥] Jose-Maria Montenegro,[†] Kirsten Schubert,[‡] Gero Göbel,[‡] Fred Lisdat,[‡] Gregor Witte,[†,*] and Wolfgang J. Parak[†,*]

[†]Fachbereich Physik and WZMW, Philipps-Universität Marburg, Marburg, Germany and, [‡]Biosystems Technology, Technical University of Applied Sciences, Wildau, Germany. [§]These authors contributed equally to this study. [∥]Present address: Department of Electronics, Nankai University, Tianjin, China.

ABSTRACT

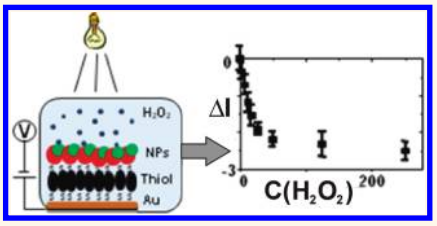

A light-addressable gold electrode modified with CdS and FePt or with CdS@FePt nanoparticles *via* an interfacial dithiol linker layer is presented. XPS measurements reveal that *trans*-stilbenedithiol provides high-quality self-assembled monolayers compared to benzenedithiol and biphenyldithiol, in case they are formed at elevated temperatures. The CdS nanoparticles in good electrical contact with the electrode allow for current generation under illumination and appropriate polarization. FePt nanoparticles serve as catalytic sites for the reduction of hydrogen peroxide to water. Advantageously, both properties can be combined by the use of hybrid nanoparticles fixed on the electrode by means of the optimized stilbenedithiol layer. This allows a light-controlled analysis of different hydrogen peroxide concentrations.

KEYWORDS: quantum dots · hydrogen peroxide · sensor · self-assembled monolayers · light-controlled detection

Most commonly, spatial resolution in electrochemical sensors is achieved by structured surfaces, such as arrays of electrodes. One alternative is addressing individual points on an unstructured electrode by light. The concept of such light-addressable electrodes has been introduced already decades ago.[1−3] Hereby, illumination of selected spots on the electrode surface generates a local photocurrent, and thus by scanning a light pointer across the sensor surface, different positions can be addressed; that is, spatially resolved measurements are possible[4] (*cf.* Figure 1a). Traditionally, such light-addressable sensors have been designed as microfabricated silicon chips, typically in doped silicon−silicon oxide/silicon nitride geometry. The essential element is a semiconductor layer, in which light-generated electron−hole pairs can be generated as local charge carriers with the light pointer.

In recent years, attempts have been reported to create similar setups, however, by placing a layer of semiconductor nanoparticles (quantum dots, QDs) on the surface of gold electrodes *via* conductive dithiols as a linker.[5,6] This approach has potentially several advantages. First, QD layers can be deposited on gold surfaces without the requirement of any microfabrication facilities. Second, due to the small size of the QDs and prevention of lateral current in the QD layer, in principle, better spatial resolution could be obtained. Third, besides semiconductor nanoparticles (QDs), other types of nanoparticles (NPs) can be added on top of the gold electrode, which could, for example, specifically trigger catalytic reactions. QDs have been characterized electrochemically.[7−11] Functionality of QD-modified gold electrodes as electrochemical sensors has been demonstrated before and also applied to the detection of enzymatic reactions.[12,13] Though attempts have been made to quantitatively optimize the QD layer on the gold surface and thus to improve sensor performance,[14] still a conclusive picture of the nanostructure of this interfacial layer is missing. In spite of the fact that in most images such NP layers are

* Address correspondence to gregor.witte@physik.uni-marburg.de, wolfgang.parak@physik.uni-marburg.de.

Received for review September 15, 2011 and accepted November 9, 2011.

Published online November 09, 2011
10.1021/nn2035582

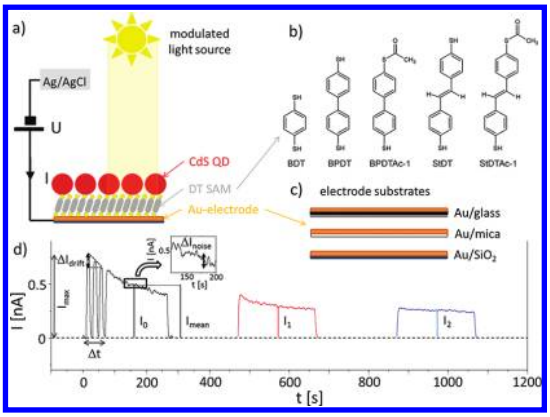

Figure 1. Experimental setup. (a) Setup of the light-controlled electrode comprising a QD layer on top of a gold electrode with an interfacial dithiol layer, an applied bias voltage, and a modulated light source. (b) Schematic illustration of the different dithiols. (c) Schematic illustration of the geometry of the different used gold substrates. (d) Photocurrent I recorded over time at fixed bias potential $U = +200$ mV.

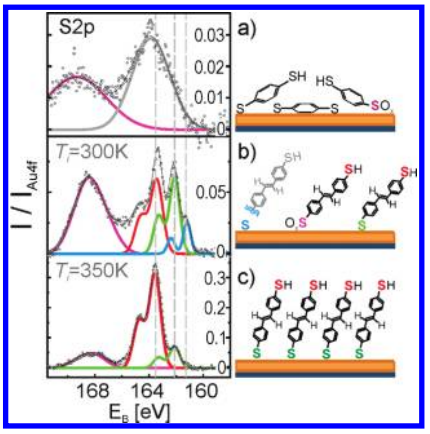

Figure 2. XPS of the different SAMs. (a–c) S2p XP spectra of the following SAMs on Au/SiO_2: (a) BDT, (b) StDT prepared by immersion at room temperature, and (c) at 350 K. The different sulfur species have been identified according to their binding energies as sulfides (AuS, blue), thiolates (AuS-R, green), thiols (R-SH, R-SAc, red), and sulfonates ($AuSO_x$, purple).

depicted as homogeneous self-assembled monolayers (SAMs), so far no detailed data exist, which would support such statement about the geometry.

In the present work, the QD–SAM–Au junction was systematically studied for the case of various dithiol SAMs adsorbed onto differently prepared gold electrodes in order to emphasize the importance of defined structures on device performance and to understand and optimize such sensors. Best device performance was obtained for a conjugated stilbenedithiol linker, which can be assembled as a structurally well-ordered monolayer by means of immersion at elevated temperature without the necessity of protection groups, while this was required for preparation at room temperature. This analysis has also to be seen in a more general context of investigating the structure of NP layers on top of plane surfaces as we demonstrate also the ability of making such layers of different materials. Besides semiconducting CdS QDs, which serve as a switch for light-controlled detection, also other NPs can be used, which for example locally catalyze reactions at the electrode surface. In the present case, we demonstrate the detection of H_2O_2 *via* catalytic degradation at the surface of FePt NPs and charge transfer from the electrode *via* the CdS QDs.

RESULTS AND DISCUSSION

Self-Assembled Dithiol Monolayers on Gold Surfaces. As the first step, electrodes were prepared by generating self-assembled layers of different dithiols (1,4-benzenedithiol (BDT), 4-4′-biphenyldithiol (BPDT), biphenyldithiol monoacetylated (BPDTAc-1), *trans*-4,4′-stilbenedithiol (StDT), and *trans*-4,4′-stilbenedithiol monoacetylated (StDTAc-1),[15] *cf.* Figure 1b) on three different Au substrates (Au/glass (with a thin Ti intermediate layer), Au/mica, Au/SiO_2, *cf.* Figure 1c). For this purpose, dithiols were dissolved at a concentration of 100 nM in dichloromethane or toluene and the Au substrates were immersed in these solutions. The amount of dithiols has been calculated to be enough to completely cover the Au surface. For characterization, XPS (X-ray photoelectron spectroscopy) was carried out at the HE-SGM synchrotron beamline of BESSY II in Berlin. All experimental protocols and several characterization measurements are described in detail in the Supporting Information.

In previous works, commonly, BDT has been used to immobilize QDs on Au electrodes,[5] although they form rather poorly ordered SAMs. Like in the case of benzenethiol,[16] their short backbone offers only a weak intermolecular stabilization, which leads to a reclined molecular orientation after adsorption on gold substrates.[17] As a consequence, the molecular film is lacking its function for anchoring the QDs provided by densely packed SAMs of upright oriented molecules with thiol groups exposed to the solution, and a noticeable oxidation of the thiolate anchoring groups takes place.

Indeed, the poor ordering of BDT SAMs is clearly evidenced by high-resolution XPS measurements (details of this analysis and about the experimental setup are given in the Supporting Information). As depicted in Figure 2a, corresponding XPS data of the sulfur region reveal an intense sulfonate signal at a binding energy of 168.5 eV, while the sulfur signals of the thiol and thiolate species are not separated, thus reflecting an inhomogeneous broadening due to disorder of the film. Largely improved ordering of SAMs has been achieved for thiols with larger but more rigid backbones such as oligophenylenes. Since dithiols potentially might bind with both thiol groups to the gold surface, protective monoacetylation was performed, permitting in turn selective anchoring; that is, only the free thiol can react with the gold surface.[15,18,19]

TABLE 1. Electrical Characterization of CdS QDs Immobilized on Top of SAMs of Different Dithiol Molecules That Were Adsorbed on Different Electrode Substrates[a]

dithiols	substrate	I_{mean} [nA]	$\tau_{drift} = (\Delta I/I_{mean})/\Delta t$ [s^{-1}]	I_{mean}/I_{noise}	$(I_0 - I_2)/I_0$ [%]
	Au/mica	0.27 ± 0.04	$(5.1 \pm 1.8) \times 10^{-2}$	5.7 ± 1.0	68.1 ± 2
BDT	Au/glass	0.67 ± 0.15	$(2.5 \pm 0.4) \times 10^{-2}$	17.3 ± 2.5	52.3 ± 2.4
	Au/SiO_2	1.56 ± 0.30	$(4.8 \pm 2.2) \times 10^{-4}$	55 ± 8	30.5 ± 4.4
BPDT	Au/mica	0.07 ± 0.02	$(4.8 \pm 1.2) \times 10^{-2}$	3.5 ± 1.1	100
	Au/glass	0.00[c]			
	Au/SiO_2	0.62 ± 0.10	$(3.8 \pm 2.4) \times 10^{-4}$	10.4 ± 1.7	32.1 ± 0.7
	Au/mica	0.11 ± 0.02	$(6.8 \pm 0.6) \times 10^{-2}$	15.5 ± 1.6	47.3 ± 1.8
BPDTAc-1[b]	Au/glass	0.3 ± 0.07	$(3.4 \pm 0.6) \times 10^{-2}$	26.7 ± 6.9	26.5 ± 4.9
	Au/SiO_2	1.76	1.3×10^{-4}	47.62	22.2
StDT	Au/mica	0.37 ± 0.07	$(2.5 \pm 0.7) \times 10^{-2}$	20.3 ± 5.6	35.6 ± 5.3
	Au/glass	1.08 ± 0.11	$(4.1 \pm 0.8) \times 10^{-2}$	40.0 ± 6.2	21.7 ± 5.2
	Au/SiO_2	1.57 ± 0.14	$(2.9 \pm 1.3) \times 10^{-4}$	48.9 ± 6.2	12.4 ± 1.1
StDTAc-1[b]	Au/mica	0.51 ± 0.12	$(1.9 \pm 0.8) \times 10^{-2}$	13.8 ± 3.1	46.6 ± 4.1
	Au/glass	1.45 ± 0.45	$(1.3 \pm 0.4) \times 10^{-2}$	38.5 ± 12.6	30.3 ± 2.3
	Au/SiO_2	2.51 ± 0.14	$(1.7 \pm 0.1) \times 10^{-4}$	137 ± 5.0	4.4 ± 0.6
StDT (heated)	Au/SiO_2	8.84 ± 0.50	$(8.4 \pm 0.5) \times 10^{-5}$	262.8 ± 15.2	1.0 ± 0.1

[a] The definition of the parameters is given in Figure 1d. All measurements have been replicated with at least two different electrodes (with the exception of BPDTAc-1 on Au/SiO_2 because the gold electrode turned out to be very fragile upon decapping), and data represent mean values with the corresponding standard deviation.. [b] The capping group had been removed after assembly of the dithiol SAM, before attachment of the QDs. [c] The photocurrent was below the detection limit.

In the present study, this strategy has been utilized for the case of BPDT by first preparing a SAM of BPDTAc-1 and, subsequently, decapping the acetate group by immersion in NaOH solution (*cf.* Supporting Information) before immobilization of the NPs. Despite a distinctly improved ordering of such dithiol SAMs (*cf.* Figure S5 of Supporting Information), the corresponding sensor characteristics have improved only little as compared to those using BDT SAMs (*cf.* Table 1). This result can be attributed to the modest conductivity of biphenyl-based SAMs (HOMO−LUMO band gap >4 eV), which in turn hampers an efficient electron transfer of the electron−hole pair from the illuminated QDs to the gold substrate. Note that this energy gap is almost independent of the number of phenyl rings because they are separated by C−C single bonds,[20] hence demonstrating that oligophenylene-based thiols are only partly conjugated.

Therefore, dithiols with fully conjugated backbones such as *trans*-stilbenes have been used instead because they exhibit a distinctly smaller HOMO−LUMO gap of only 2.14 eV.[21] In order to avoid simultaneous anchoring of both thiols of StDT, which again results in a partial oxidation and a poor film ordering (as indicated by corresponding XPS data shown in Figure 2b), also StDTAc-1 was used (for synthesis and film characterization, see the Supporting Information). After decapping, highly ordered StDT SAMs were obtained, which enable the fabrication of QD-based sensors with largely improved device performance (see detailed discussion in the next section and data in Table 1). In contrast to the partly conjugated SAMs, acetylated stilbenedithiol was found to be rather metastable and exhibits a rapid photo-oxidation within of several hours and, therefore, requires a quick processing after its synthesis.

In order to provide a more robust method to prepare highly ordered StDT SAMs, another approach has been tested. Guided by previous studies that reported a largely improved ordering of organothiol SAMs by immersion at elevated temperature or annealing in nitrogen atmosphere,[22,23] StDT SAMs were alternatively prepared by immersing Au/SiO_2 samples in thiol solution at about 350 K. Surprisingly, this procedure yielded excellent films even for nonprotected stilbenedithiols. Comparing the corresponding XPS data (see Figure 2c) with those obtained for SAMs of acetylated stilbenedithiols after decapping (*cf.* Figure S6c of Supporting Information), even further improved film quality has been assessed. This is evidenced by distinctly enhanced intensity ratios of the thiol-to-gold and the thiol-to-thiolate signals, which reflect a denser molecular packing and a more upright orientation. The latter finding has also been confirmed directly by near-edge X-ray absorption fine structure (NEXAFS) measurements (see Supporting Information, Figure S7), which yield a molecular tilt angle of 62° with respect to the surface plane.

Electrical Characterization of Quantum Dots Layers on Top of Self-Assembled Monolayers of Conductive Dithiols. In the next step, the influence of the various SAMs on the electrical properties of the light-addressable sensor has been investigated. For this purpose, CdS QDs were immobilized on top of the SAM-covered gold electrodes by immersion. CdS,[24] FePt,[25,26] and CdS@FePt[26,27] NPs have been synthesized according to previously published protocols. CdS@FePt NPs are hybrid NPs in which a bleb of CdS has been grown on spherical FePt

NPs.[26,27] Electrical characterization of the NP-covered electrodes was performed as previously described elsewhere.[14] Optical and structural data are shown in the Supporting Information (Figures S1−S3).

The experimental setup is depicted in Figure 1a. All experimental protocols and several characterization measurements are described in detail in the Supporting Information. The modulated light source was periodically switched on and off, and the photocurrent I was recorded during on-periods at fixed bias potential $U = +200$ mV in 0.1 M phosphate buffer solution (pH = 7.5) *versus* time. Four parameters were extracted from each photocurrent trace $I(t)$ as previously described[14] and depicted in Figure 1d: the average photocurrent I_{mean} (while turning on and off the light source in the first part of cylce), the current decay rate $\tau_{drift} = (\Delta I_{drift}/I_{mean})/\Delta t$, which is a measure for drifts in photocurrent ΔI_{drift}, the signal-to-noise ratio $I_{mean}/\Delta I_{noise}$, and the loss in photocurrent amplitude $(I_0 - I_2)/I_0$ after rinsing of the sensor surface with water. Here I_0 denotes the mean current (at the "on" interval at the end of each cycle) before any rinsing step and I_2 the mean current after the second rinsing step. Experimental details are described in the Supporting Information. It can be seen in Figure 1d that the loss of photocurrent during the second rinsing step is considerably lower than after the first rinsing step. This suggests that after several rinsing steps a stable equilibrium can be reached. The results obtained for sensors made from the various dithiols and different gold electrodes are summarized in Table 1. In all cases, electrical performance of the sensor was found to be best for Au/SiO_2 substrates. Note that there was no photocurrent for SAM-modified substrates without QDs (*cf.* Supporting Information Figure S15d). With one exception, Au/glass substrates lead to slightly better performance than Au/mica. We speculate that the Au/SiO_2 substrates were cleaner than the Au/glass substrates. The former electrodes were used for immersion shortly after their preparation, whereas the latter ones had been stored for months before usage. The Au/mica substrates were certainly the locally smoothest samples but have only a limited mechanical stability and tended to peel off during operation of the electrochemical cell; that is, adhesion of the gold was found to be rather poor.

Electrical performance depends directly on the quality of the SAMs, as this is also crucial for the attachment of the QD layers. XPS data have demonstrated to be rather defective SAMs in the case of BDT and BPDT. This goes hand in hand with poor sensor performance, that is, low signal-to-noise ratio and high reduction of the photocurrent after rinsing. SAM creation with capped dithiols (after decapping) resulted in clearly improved electrical characteristics (BPDTAc-1 *versus* BPDT and StDTAc-1 *versus* StDT). StDTAc-1 gave improved photocurrent measurements compared to BPDTAc-1, which can be attributed to its smaller

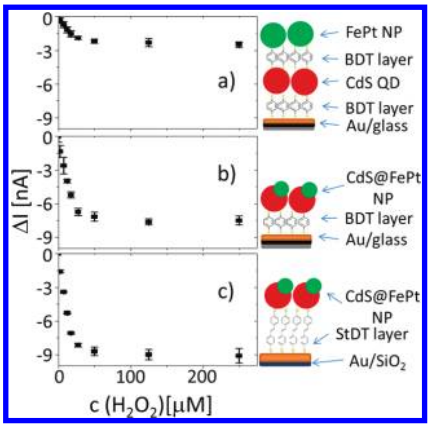

Figure 3. H_2O_2 detection in the different assemblies. (a) Alternating layers of CdS and FePt NPs and (b,c) CdS@FePt NPs were immobilized *via* dithiol SAMs (BDT (a,b), heated StDT (c)) on top of Au electrodes. Electrodes were constantly illuminated with a modulated light source, and the amplitude I of the photocurrent was detected at fixed applied bias voltage $U = -200$ mV. Different concentrations of H_2O_2 were added to the buffer solution (pH = 7.5) on top of the electrode. Changes in photocurrent due to addition of H_2O_2 are plotted *versus* the H_2O_2 concentration for the three depicted geometries.

HOMO−LUMO energy gap. Generally, the acetylation improves the ordering of dithiol SAMs, as it suppresses a reclined molecular orientation accompanied by partial oxidation of thiolate anchoring units. This is decisive, as oxo-functions have been demonstrated to act as electron traps which distinctly reduce the charge transport through SAMs[28] and therefore have to be avoided. Best electrical performance was achieved with SAMs of StDT created at elevated temperatures (on Au/SiO_2 substrates). This corresponds to a SAM with the highest coverage and upright packing yielding the fewest defects as indicated by XPS data. It also has the lowest loss of photocurrent upon rinsing, which presumably is due to loss of QDs for the SAMs. We thus conclude that the highly ordered structure of the StDT layer with fully reactive thiol groups exposed to the solution provides obviously good conditions for a defined immobilization of CdS QDs. The QDs have to bind to the thiol group by exchanging the ligand from their preparation on their surface with the surface group on the Au electrode. Thus, surface disorder and oxidized species on the surface would diminish the stable anchoring on the electrode, which is the reason for the best performance of StDT SAMs generated at high temperatures.

Sensing of H_2O_2. In a final step, we wanted to transfer the better understanding of the QD layer−SAM−Au electrode interface to improve sensing characteristics. Hereby, we also wanted to make use of the possibility of attaching different types of colloidal NPs. In the present study, we have chosen FePt NPs as the catalytic element since platinum is known for its electrocatalytic activity for hydrogen peroxide conversion, particularly reduction ($H_2O_2 + 2H^+ + 2e^- \rightarrow 2\ H_2O$), and as a

synthesis protocol for CdS@FePt has been readily available.[26,27] Hydrogen peroxide detection is an important analytical task both for physiological and nonphysiological applications.[29−31]

Addition of FePt NPs to the CdS NPs on the Au surface should thus facilitate sensing of H_2O_2. Dose−response curves of the dependence of the photocurrent from hydrogen peroxide were recorded. Experimental details and characterization measurements are shown in the Supporting Information. In fact, no response of the photocurrent to H_2O_2 was found for either only CdS NPs or only FePt NPs (no photocurrent at all) immobilized at the Au electrode surface (*cf.* Supporting Information). This corresponds to previous findings with CdSe/ZnS NPs on electrodes, which also did not provide a surface for efficient hydrogen peroxide conversion.[13] However, the combination of CdS and FePt NPs on the Au electrode surface leads to a photocurrent, which amplitude depends on the H_2O_2 concentration in the buffer above the electrode (*cf.* Figure 3). Data about dependence on bias voltage and pH are shown in the Supporting Information. As mentioned above, reduction of H_2O_2 involves H^+ and e^-, which account for dependence on pH and bias potential, respectively. Thus, it is found that reduction is preferred in the acidic pH region (pH 5) and can be facilitated by decreasing the electrode potential from −0.2 to −0.6 V *vs* Ag/AgCl.

For combining CdS and FePt NPs, we have actually employed three different geometries. In the first case (Figure 3a), CdS NPs were attached on top of BDT SAMs on Au/glass substrates, which is compatible to conditions in our previous reports.[14] FePt NPs were added on top *via* an additional BDT layer. Please note that images are not drawn to scale and that, according to the XPS data, the structure is depicted only schematically. Clearly, a dependence of the photocurrent on H_2O_2 concentration (up to *ca.* 100 μM) could be observed.

Modern synthesis protocols also allow for the production of hybrid NPs, such as CdS NPs grown on top of FePt NPs.[26,27] In this way, a combination of two materials with different functionalities in one particle is possible. Figure 3b shows the resulting sensor response of CdS@FePt NPs immobilized *via* BDT on top of Au/glass electrodes. In comparison to the mixed assembly of CdS and FePt NPs (Figure 3a), a 2−3 times higher response to H_2O_2 could be observed. This can be easily understood. Upon reduction of H_2O_2, electrons need to be transferred from the FePt NPs (the location where the reduction takes place) to H_2O_2. Source of the electrons is the CdS QDs, which in turn receive electrons from the Au electrode *via* the conductive dithiol SAM. Effectively, electrons are injected from the Au electrode for reduction of H_2O_2, which results in a photocurrent with negative sign (*cf.* Figure 1a and Figure 3). In the case of CdS@FePt NPs, electrons can flow directly from the CdS to the FePt domain without having to cross an external interface. In the case of coassembly of CdS and FePt NPs, electrons need to be transferred from the CdS NPs to the FePt NPs *via* BDT molecules, which reduces the intensity of the photocurrent.

As indicated by the XPS characterization of the various dithiol SAMs and the electrical device characterization, best performance would be expected using StDT as linker and Au/SiO_2 as substrate. Dose−response curves of the photocurrent *versus* H_2O_2 concentration were similar to that recorded with BDT on top of Au/glass but had ∼20% improvement in photocurrent response (*cf.* Figure 3b,c). The error bars of the photocurrent measurements from typically three electrodes at low H_2O_2 concentrations also reveal that better signal-to-noise ratio for StDT is achieved (*cf.* Figure 3b,c). Consequently, StDT monolayers on top of Au/SiO_2 substrates result in a higher sensitivity for hydrogen peroxide detection and would allow for a lower H_2O_2 concentration as detection limit. Thus, this configuration offers the best geometry used in the present study, which goes far beyond the previously used setups.

CONCLUSIONS

It is demonstrated that the quality of interfacial dithiol films used to immobilize a QDs layer on gold electrodes has a severe influence on the electrical properties of a light-controlled sensor. The use of dithiol linkers with high conductivity and their assembly to a highly ordered, densely packed film with upright molecular orientation is of key importance in order to avoid partial oxidation of thiolate anchoring units. While an improved structural ordering of dithiol SAMs is achieved by first capping one of the thiol groups (*e.g.*, monoacetylation) followed by decapping after SAM formation, this strategy is complicated by a rapid photo-oxidation of the acetylated group in the case of low band gap materials such as the presently studied stilbenedithiols.

However, well-ordered StDT films have been achieved by immersion at elevated temperature, without the use of capping groups. Corresponding sensors reveal an enhancement of the photocurrent by more than an order of magnitude as well as a largely improved rinsing stability compared to devices based on the commonly used BDT. In this way, the ordered structure with fully reactive thiol groups exposed to the solution side improves the anchoring of the QDs.

Furthermore, we have demonstrated that inclusion of other types of NPs facilitates new detection modalities. In the present case, FePt NPs have been used as catalytic sites for the conversion of H_2O_2. These particles can be co-immobilized with the QDs, or more advantageously hybrid CdS@FePt NPs have been used

to combine the properties of photoexcitation with the catalytic activity. Thus, a photoelectrochemical analysis of H_2O_2 becomes feasible. This can be the basis of a set of biosensors involving enzymes with H_2O_2 as product.

MATERIALS AND METHODS

Preparation of Gold Electrodes. For the realization of the light-addressable sensor, three different kinds of gold substrates were prepared that have been utilized as electrodes. Initially, commercially available Au-coated glass slides (Au/glass) had been used, which were compared with self-made gold electrodes consisting either of Au layers evaporated onto mica sheets (Au/mica) or Au films sputtered onto oxidized Si wafers (Au/SiO_2).

Au/Glass. First, 100 nm of gold was evaporated on glass slides with the assistance of a 20 nm Ti adhesion layer. The Au/glass substrates were obtained from Institut für Mikrotechnik Mainz GmbH (iMM). These Au/glass slides were initially protected with a photoresist to avoid oxidation. The removal of the photoresist was done by sonication of the Au/glass substrates in toluene, ethanol, and acetone sequentially for 5 min each. To further remove impurities and leftover oxides, the Au surface was cleaned by cyclic voltammetry (CV) in 1 M NaOH (−0.8 V to +0.2 V) and 0.5 M H_2SO_4 (−0.2 V to +1.6 V). CV was done only with Au/glass. The other two electrode systems (Au/mica, Au/SiO_2) were used as received, as they were freshly prepared.

Au/Mica. Substrates were prepared by evaporating about 150 nm gold (99.995%, Chempur) at 540 K under high vacuum conditions ($\sim 10^{-8}$ mbar) onto freshly cleaved mica sheets, which had been heated to 525 K for 24 h before deposition to remove contaminations and residual crystal water. After deposition, the Au/mica substrates were flame-annealed in a protective nitrogen atmosphere for about 1 min at temperatures of 950 K to enhance crystallinity and reduce the roughness. This procedure yields high-quality Au films with atomically flat terraces of several hundred nanometers, exhibiting a (111) surface orientation that is well-suited for STM measurements.[32] Unfortunately, these substrates appear to be unstable during operation in the electrochemical cell since the gold films were found to peel off from the mica support.

Au/SiO_2. Substrates consist of gold films that were sputtered onto polished Si(100) wafers (Silchem). Before sputter-deposition of gold (99.98%) under argon atmosphere (POLARON sputter coater), the wafers which are covered with a native oxide layer were rinsed thoroughly with acetone and 2-propanol and subsequently dried in a nitrogen stream. To avoid electrochemical side reaction in the electrochemical cell, no adhesion layers (like Ti or Cr) were used. As a result, thick gold films (≥30 nm) were found to peel off from the wafers during the decapping procedure by immersion in NaOH solution (see below). This problem could be avoided by preparing ultrathin gold films with a thickness of only 14 nm.

Using atomic force microscopy (Agilent SPM5500), the surface morphology and roughness of the various gold substrates was characterized. In fact, Au/mica reveals atomically flat regions extending laterally over several hundred nanometers together with distinct steps of more than 10 nm between individual crystalline grains, hence yielding an overall mesoscopic waved surface. The other gold surfaces exhibit a nanogranular morphology with rms roughness values of about 3.5 nm for Au/glass and less than 2 nm for Au/SiO_2, which reflects the outstanding quality of the latter gold substrate.

Photoelectron Spectroscopy. The adsorption and chemical properties of the various self-assembled monolayers (SAMs) were characterized by means of high-resolution synchrotron-based X-ray photoelectron spectroscopy (XPS). Additional near-edge X-ray absorption fine structure (NEXAFS) measurements were carried out for StDT SAMs to obtain complementary information about the molecular orientation. All of these measurements were performed at the HE-SGM dipole beamline of the synchrotron storage ring BESSY II in Berlin (Germany). The used UHV end-station is equipped with a load-lock system that enables quick sample transfer. The XP spectra were recorded at a base pressure $p \leq 1 \times 10^{-9}$ mbar with a hemispherical energy analyzer (Scienta R3000) at an incident photon energy of 350 eV and monochromator settings (slit width) that enable an energy resolution of about 0.3 eV. All measured photoelectron binding energies have been referenced to the simultaneously recorded Au $4f_{7/2}$ peak (84.0 eV) of the substrate. Linear polarized synchrotron light (polarization factor 92%) was employed to measure the carbon edge NEXAFS spectra, which were acquired in partial electron yield mode using a channel plate detector operated with a retarding field. The NEXAFS raw data have been normalized in a multistep procedure by considering the incident photon flux and the background signal of the clean substrate.[33]

Signal-to-Noise and Drift Analysis of Photocurrent. To check the stability and resolution of the system, characterization measurements were performed. All of the measurements were recorded in 0.1 M phosphate buffer solution at pH 7.5. A constant bias potential of $U = +200$ mV was applied in all measurements. A bias potential of +200 mV was selected, as this potential had been used for the stability characterization of these kinds of electrodes in our previous work.[14] Note that this is a different potential than that used for H_2O_2 detection. Concerning the Au electrode preparation, all of the Au substrates had been immersed in 10 μM solutions of CdS QDs. For each system, at least two electrodes were tested. The Au/SiO_2 substrates were very fragile in the decapping solution of NaOH and ethanol. For characterization, a 10 s pulse of modulated light with a power $P_{illum} = 23$ mW was focused (light on) on the CdS QDs immobilized on top of the Au substrate (CdS/Au) to a spot size of approximately 2.5 mm^2. In a next period, light was switched off (light off) for 10 s. This process was repeated three times. After that, the CdS/Au substrate was illuminated with modulated light for about 200 s. The light on and light off cycles were controlled by a mechanical shutter. The current decay rate due to drift current τ_{drift} is defined, as depicted in Figure 1d, as the reduction of photocurrent under illumination within a time frame $\Delta t = 60$ s as $(\Delta I_{drift}/I_{max})/\Delta t$. I_{max} is the maximum amplitude of the photocurrent observed for each system. Signal-to-noise ratio ($I_{mean}/\Delta I_{noise}$): The light source was turned on for about 200 s continuously, and from the resulting photocurrent response, the mean current I_{mean} and the fluctuations in the current ΔI_{noise} were determined. The signal-to-noise ratio is defined as $I_{mean}/\Delta I_{noise}$. Rinsing degradation in photocurrent: Rinsing degradation in photocurrent was defined as the loss of photocurrent while rinsing the electrochemical cell two times with water (*cf.* Figure 1d). The cycle in Figure 1d was repeated three times. After each cycle, the electrochemical cell was rinsed: the phosphate buffer solution was taken out of the Teflon tank, water was poured inside the Teflon tank, water was taken out, and phosphate buffer solution was poured in again. I_0 is the mean current without any rinsing step, I_1 the mean current after the first rinsing step, and I_2 the mean current after the second rinsing step. The loss in photocurrent during the two rinsing steps was then calculated as $(I_0 - I_2)/I_0 \times 100\%$. All raw data are shown in the Supporting Information (Figure S10), and results are summarized in Table 1.

Acknowledgment. This work was supported in part by the German Research Foundation (DFG, Grant PA 794/3-1 to W.J.P. and LI706/2-1 to F.L.) and by the European Commission (EC, grant Nandiatream to W.J.P.). This work was partly funded by National Natural Science Foundation of China (Grant No.61001056) and Natural Science Foundation of Tianjin, China (Grant No.10JCZDJC15300) (to Z.Y.). W.K. acknowledges financial support by the HEC Pakistan/DAAD Germany. The authors are grateful to Dr. Abbasi Azhar for help in the nanoparticle synthesis and for recording the TEM images. We acknowledge the Helmholtz-Zentrum Berlin - Electron

storage ring BESSY II for provision of synchrotron radiation at beamline HE-SGM and travel support.

Supporting Information Available: Additional characterization of the various SAMs, synthesis of nanoparticles and dithiols, electrode preparation, and electrochemical characterization. This material is available free of charge *via* the Internet at http://pubs.acs.org.

REFERENCES AND NOTES

1. Engström, O.; Carlsson, A. Scanned Light Pulse Technique for the Investigation of Insulator-Semiconductor Interfaces. *J. Appl. Phys.* **1983**, *54*, 5245–5251.
2. Hafeman, D. G.; Parce, J. W.; McConnell, H. M. Light-Addressable Potentiometric Sensor for Biochemical Systems. *Science* **1988**, *240*, 1182–1185.
3. Licht, S.; Myung, N.; Sun, Y.; Light Addressable, A Photoelectrochemical Cyanide Sensor. *Anal. Chem.* **1996**, *68*, 954–959.
4. Parak, W. J.; Hofmann, U. G.; Gaub, H. E.; Owicki, J. C. Lateral Resolution of Light Addressable Potentiometric Sensors: An Experimental and Theoretical Investigation. *Sens. Actuators, A* **1997**, *63*, 47–57.
5. Stoll, C.; Kudera, S.; Parak, W. J.; Lisdat, F. Quantum Dots on Gold:Electrodes for Photoswitchable Cytochrome *c* Electrochemistry. *Small* **2006**, *2*, 741–743.
6. Katz, E.; Zayats, M.; Willner, I.; Lisdat, F. Controlling the Direction of Photocurrents by Means of CdS Nanoparticles and Cytochrome *c*-Mediated Biocatalytic Cascades. *Chem. Commun.* **2006**, 1395–1397.
7. Gaponik, N.; Poznyak, S. K.; Osipovich, N. P.; Shavel, A.; Eychmüller, A. Electrochemical Probing of Thiol-Capped Nanocrystals. *Microchim. Acta* **2008**, *160*, 327–334.
8. Poznyak, S. K.; Osipovich, N. P.; Shavel, A.; Talapin, D. V.; Gao, M.; Eychmüller, A.; Gaponik, N. Size-Dependent Electrochemical Behavior of Thiol-Capped CdTe Nanocrystals in Aqueous Solution. *J. Phys. Chem. B* **2005**, *109*, 1094–1100.
9. Kucur, E.; Riegler, J.; Urban, G. A.; Nann, T. Determination of Quantum Confinement in CdSe Nanocrystals by Cyclic Voltammetry. *J. Chem. Phys.* **2003**, *119*, 2333–2337.
10. Kucur, E.; Bücking, W.; Arenz, S.; Giernoth, R.; Nann, T. Heterogeneous Charge Transfer of Colloidal Nanocrystals in Ionic Liquids. *ChemPhysChem* **2006**, *7*, 77–81.
11. Gill, R.; Zayats, M.; Willner, I. Semiconductor Quantum Dots for Bioanalysis. *Angew. Chem., Int. Ed.* **2008**, *47*, 7602–7625.
12. Stoll, C.; Gehring, C.; Schubert, K.; Zanella, M.; Parak, W. J.; Lisdat, F. Photoelectrochemical Signal Chain Based on Quantum Dots on Gold-Sensitive to Superoxide Radicals in Solution. *Biosens. Bioelectron.* **2008**, *24*, 260–265.
13. Schubert, K.; Khalid, W.; Yue, Z.; Parak, W. J.; Lisdat, F. Quantum-Dot-Modified Electrode in Combination with NADH-Dependent Dehydrogenase Reactions for Substrate Analysis. *Langmuir* **2010**, *26*, 1395–1400.
14. Yue, Z.; Khalid, W.; Zanella, M.; Abbasi, A. Z.; Pfreundt, A.; Rivera-Gil, P.; Schubert, K.; Lisdat, F.; Parak, W. J. Evaluation of Quantum Dots Applied as Switchable Layer in a Light-Controlled Electrochemical Sensor. *Anal. Bioanal. Chem.* **2010**, *396*, 1095–1103.
15. Niklewski, A.; Azzam, W.; Strunskus, T.; Fischer, R. A.; Wöll, C. Fabrication of Self-Assembled Monolayers Exhibiting a Thiol-Terminated Surface. *Langmuir* **2004**, *20*, 8620–8624.
16. Käfer, D.; Bashir, A.; Witte, G. Interplay of Anchoring and Ordering in Aromatic Self-Assembled Monolayers. *J. Phys. Chem. C* **2007**, *111*, 10546–10551.
17. Joo, S. W.; Han, S. W.; Kim, K. Adsorption of 1,4-Benzenedithiol on Gold and Silver Surfaces: Surface-Enhanced Raman Scattering Study. *J. Colloid Interface Sci.* **2001**, *240*, 391–399.
18. Tour, J. M.; Jones, L.; Pearson, D. L.; Lamba, J. J. S.; Burgin, T. P.; Whitesides, G. M.; Allara, D. L.; Parikh, A. N.; Atre, S. V. Self-Assembled Monolayers and Multilayers of Conjugated Thiols, α,ω-Dithiols, and Thioacetyl-Containing Adsorbates: Understanding Attachments between Potential Molecular Wires and Gold Surfaces. *J. Am. Chem. Soc.* **1995**, *117*, 9529–9534.
19. Shaporenko, A.; Elbing, M.; Baszczyk, A.; von Hänisch, C.; Mayor, M.; Zharnikov, M. Self-Assembled Monolayers from Biphenyldithiol Derivatives: Optimization of the Deprotection Procedure and Effect of the Molecular Conformation. *J. Phys. Chem. B* **2006**, *110*, 4307–4317.
20. Bashir, A.; Käfer, D.; Müller, J.; Wöll, C.; Terfort, A.; Witte, G. Selenium as a Key Element for Highly Ordered Aromatic Self-Assembled Monolayers. *Angew. Chem., Int. Ed.* **2008**, *47*, 5250–5252.
21. Saltiel, J.; Khalil, G. E.; Schanze, K. *trans*-Stilbene Phosphorescence. *Chem. Phys. Lett.* **1980**, *70*, 233–235.
22. Cyganik, P.; Buck, M.; Strunskus, T.; Shaporenko, A.; Wilton-Ely, J.; Zharnikov, M.; Wöll, C. Competition as a Design Concept: Polymorphism in Self-Assembled Monolayers of Biphenyl-Based Thiols. *J. Am. Chem. Soc.* **2006**, *128*, 13868–13878.
23. Qi, Y.; Liu, X.; Hendriksen, B. L. M.; Navarro, V.; Park, J. Y.; Ratera, I.; Klopp, J. M.; Edder, C.; Himpsel, F. J.; Frechet, J. M. J.; *et al.* Influence of Molecular Ordering on Electrical and Friction Properties of ω-(*trans*-4-Stilbene)Alkylthiol Self-Assembled Monolayers on Au(111). *Langmuir* **2010**, *26*, 16522–16528.
24. Kudera, S.; Carbone, L.; Casula, M. F.; Cingolani, R.; Falqui, A.; Snoeck, E.; Parak, W. J.; Manna, L. Selective Growth of PbSe on One or Both Tips of Colloidal Semiconductor Nanorods. *Nano Lett.* **2005**, *5*, 445–449.
25. Sun, S.; Murray, C. B.; Weller, D.; Folks, L.; Moser, A. Monodisperse FePt Nanoparticles and Ferromagnetic FePt Nanocrystal Superlattices. *Science* **2000**, *287*, 1989–1992.
26. Zanella, M.; Falqui, A.; Kudera, S.; Manna, L.; Casula, M. F.; Parak, W. J. Growth of Colloidal Nanoparticles of Group II–VI and IV–VI Semiconductors on Top of Magnetic Iron-Platinum Nanocrystals. *J. Mater. Chem.* **2008**, *18*, 4311–4317.
27. Gu, H.; Zheng, R.; Zhang, X. X.; Xu, B. Facile One-Pot Synthesis of Bifunctional Heterodimers of Nanoparticles: A Conjugate of Quantum Dot and Magnetic Nanoparticles. *J. Am. Chem. Soc.* **2004**, *126*, 5664–5665.
28. Wang, Z. H.; Käfer, D.; Bashir, A.; Götzen, J.; Birkner, A.; Witte, G.; Wöll, C. Influence of OH groups on Charge Transport Across Organic–Organic Interfaces: A Systematic Approach Employing an "Ideal" Device. *Phys. Chem. Chem. Phys.* **2010**, *12*, 4317–4323.
29. Krylov, A. V.; Adamzig, H.; Walter, A. D.; Löchel, B.; Kurth, E.; Pulz, O.; Szeponik, J.; Wegerich, F.; Lisdat, F. Parallel Generation and Detection of Superoxide and Hydrogen Peroxide in a Fluidic Chip. *Sens. Actuators, B* **2006**, *119*, 118–126.
30. Guo, S. J.; Dong, S. J. Biomolecule–Nanoparticle Hybrids for Electrochemical Biosensors. *TrAC, Trends Anal. Chem.* **2009**, *28*, 96–109.
31. Karyakin, A. A. Prussian Blue and Its Analogues: Electrochemistry and Analytical Applications. *Electroanalysis* **2001**, *13*, 813–819.
32. Merzlikin, S. V.; Tolkachev, N. N.; Strunskus, T.; Witte, G.; Glogowski, T.; Wöll, C.; Grünert, W. Resolving the Depth Coordinate in Photoelectron Spectroscopy - Comparison of Excitation Energy Variation *vs*. Angular-Resolved XPS for the Analysis of a Self-Assembled Monolayer Model System. *Surf. Sci.* **2008**, *602*, 755–767.
33. Reiss, S.; Krumm, H.; Niklewski, A.; Staemmler, V.; Wöll, C. The Adsorption of Acenes on Rutile TiO_2(110): A Multi-Technique Investigation. *J. Chem. Phys.* **2002**, *116*, 7704–7713.